Journal of Systems Engineering and Electronics
Vol. 35, No. 3, June 2024, pp.793 – 804

Relative orbit determination algorithm of space targets with passive observation

DAI Chenchao[1], QIANG Hongfu[1], ZHANG Degang[2,3], HU Shaolei[4], and GONG Baichun[2,*]

1. Zhijian Laboratory, Rocket Force University of Engineering, Xi'an 710025, China;
2. College of Astronautics, Nanjing University of Aeronautics and Astronautics, Nanjing 210016, China;
3. China Flight Test Research Institute, Xi'an 710089, China;
4. Beijing Institute of Control and Electronic Technology, Beijing 100038, China

Abstract: Angles-only relative orbit determination for space non-cooperative targets based on passive sensor is subject to weakly observable problem of the relative state between two spacecraft. Previously, the evidence for angles-only observability was found by using cylindrical dynamics, however, the solution of orbit determination is still not provided. This study develops a relative orbit determination algorithm with the cylindrical dynamics based on differential evolution. Firstly, the relative motion dynamics and line-of-sight measurement model for near-circular orbit are established in cylindrical coordinate system. Secondly, the observability is qualitatively analyzed by using the dynamics and measurement model where the unobservable geometry is found. Then, the angles-only relative orbit determination problem is modeled into an optimal searching frame and an improved differential evolution algorithm is introduced to solve the problem. Finally, the proposed algorithm is verified and tested by a set of numerical simulations in the context of high-Earth and low-Earth cases. The results show that initial relative orbit determination (IROD) solution with an appropriate accuracy in a relative short span is achieved, which can be used to initialize the navigation filter.

Keywords: angles-only measurement, relative orbit determination, cylindrical coordinate, differential evolution.

DOI: 10.23919/JSEE.2024.000051

1. Introduction

Currently, the near Earth orbital environment becomes quite complicated as the development of space technology and the significant increasing of space launching activities. The safety threat from huge number of non-cooperative space targets such as space debris, failed satellites, and malfunction satellites increases rapidly. For example, China's Yunhai-1-02 satellite was hit by unknown space targets and then disintegrated in March 2021. At least 21 pieces of debris larger than 10 cm from this collision were detected by US space force. Thus, in order to guarantee the safety of the orbit space, it is crucial to develop space situational awareness technology to conduct detection, orbit determination, cataloging, tracking and other operations for the space non-cooperative targets. However, the deployment of global ground-based tracking platforms for space situational awareness is not cost-efficient. Therefore, it is a realistic requirement to develop space-based situational awareness systems.

Generally, satellite-based sensors can be used for relative measurement of space non-cooperative targets include microwave radar, light detection and ranging (LIDAR), and optical camera. Among them, microwave radar is almost impossible to be equipped on micro and small-sized satellites because of the complex systems, high cost, high-energy consumption, and other disadvantages. LIDAR does not have the disadvantages of large volume and high power consumption, but its coverage spans only kilometers. In contrary, the passive optical camera has advantages of small size, light weight, low power consumption, full autonomy, and the invisibility of passive measurement, so it has become one of the main recommended sensors for space-based detection [1]. "ARGON" [2] and "AVANTI" [3] projects performed some on-orbit experiments with angles-only relative navigation, and "DEOS" [4], and "Phoenix" [5] have planned to perform angles-only relative navigation tests.

However, the passive optical cameras can only measure the line-of-sight (LOS) information of the target without range information, which leads to the well-known observability problem of angles-only orbit determination [1,6]. In order to solve this problem, many researches have been done from different perspectives in the past decades. Generally speaking, the solutions to the angles-only problem can be divided into four types: (i) multi-LOS scheme; (ii) orbit maneuver scheme; (iii) sen-

Manuscript received March 08, 2023.
*Corresponding author.
This work was supported by the National Natural Science Foundation of China (12272168) and the Foundation of Science and Technology on Space Intelligent Control Laboratory (HTKJ2023KL502015).

sor offset scheme; (iv) complicated dynamics scheme.

The multi-LOS scheme, including the multi-spacecraft cooperative mode and multi-sensor on one spacecraft cooperation mode has been researched to solve the observability problem. Chen et al. examined the double-LOS-based algorithm of the angles-only problem for autonomous rendezvous, where the feasibility of introducing a baseline to the problem was analyzed [7]. Hippelheuser et al. [8,9] and Tasif et al. [10] presented a new angles-only measurement model by utilizing a constellation of observing nodes. LeGrand et al. investigated an angles-only relative orbit determination algorithm based on binocular stereoscopic vision [11]. Wang et al. analyzed the two-sensor scheme for the angles-only problem during space pursuit-evasion game [12]. Andrews et al. analyzed the hybrid scheme using both space-based and ground-based sensors for geosynchronous orbit catalog maintenance [13].

The orbit maneuver scheme uses the maneuver to change the status of coasting flight to provide the observability for angles-only measurement. Chari [6] proposed the idea of orbit maneuvers to improve observability. Woffinden et al. investigated the angles-only observable criterion from the geometric viewpoint for autonomous rendezvous and developed explicit solutions to calculate the maneuvers with optimal observability for simple sets of initial conditions [14,15]. Alternatively, Grzymisch et al. mathematically derived a set of optimal observability criterion for maneuver scheme and proposed an optimal rendezvous guidance algorithm with enhanced observability for angles-only relative navigation [16−18]. Anjaly et al. [19] proposed the idea of using orbit maneuver information to estimate the distance, and studied the maneuver method with optimal observability. The angles-only relative navigation problem is also studied from the view of orbit maneuvers scheme [20−24].

Sensor offset scheme was first demonstrated by Klein et al. [25] that the lever arm effect of the optical sensor offset from the center of mass of the vehicle provides the angles-only observability. Geller et al. [26] derived the relative orbit determination solution when the angles-only sensor offset provides observability. Gong et al. analytically analyzed the performance of Perez's solution by using covariance analysis techniques and developed an improved algorithm for the problem with augmented state [27,28]. Gong et al. [29] also analytically analyzed the observability criterion for this scheme. Christensen et al. [30] confirmed the improvement of spin-assisted effectiveness to the angles-only observability when the sensor offset is considered. The sensor offset approach is limited by the fact that the offset from the center-of-mass cannot be long enough to provide sufficient observability when the separation between two spacecraft are not very close.

The multi-LOS scheme and orbit maneuver scheme for angles-only problem have "hard" cost including extra fuel consumption or extra sensor/satellite while the sensor offset scheme is generally applicable for close range cases. Alternatively, other works try to solve observability problem from the perspective of complicated dynamics with the "soft" cost of calculating. Some researchers use nonlinear Cartesian dynamics to provide observability [31−36]. Gong et al. developed a fast orbit determination algorithm by exploiting a deep neural network based on nonlinear Cartesian dynamics with J2 and three-body perturbations [37]. Some researchers studied the problem by using the relative orbit elements dynamics [38−44] where the weakly and strongly observable components of the relative orbit state were decoupled. Some other works studied the problem by using curvilinear dynamics. For example, Grzymisch et al. examined the angles-only relative navigation when the relative dynamics in rotating spherical frame centered at the target [45]. Geller et al. studied the problem based on the relative dynamics in Earth-centered spherical coordinates [46] and subsequently Perez et al. developed a non-iterative orbit determination solution with J2 perturbations, where two orbits could be obtained from LOS measurements [47]. Recently, Geller et al. examined angles-only observability in an Earth-centered cylindrical coordinate system that the full state was demonstrated to be observable using numerical simulations [48−50]. Gong et al. presented an angles-only relative navigation scheme based on the cylindrical dynamics for long-endurance applications [51].

In summary, each solution has its own advantages and limitations. As to the long-range missions for space-based situational awareness, the angles-only scheme based on complicated dynamics is a good choice. However, the classical nonlinear relative orbit dynamics modeled in Cartesian coordinates are not sensitive enough to capture the orbit curvature from the noised measurements. The utilization of curvilinear dynamics for angles-only problem is a quite promising solution. Thus, the angles-only initial relative orbit determination using cylindrical relative dynamics, which has strong capability of orbital curvature capture, is studied in this paper. The angles-only problem is modeled into an optimal problem and an improved differential evolution algorithm is introduced to solve it. This solution can be used to initialize the filter for real-time navigation and tracking.

The rest of this paper is organized as follows. The relative motion dynamics model and LOS measurement model in cylindrical coordinate system are established in Section 1 and Section 2, and then the observability analysis of relative orbit state is conducted in Section 3. After that, the angles-only initial relative orbit determination

frame is modeled in Section 4 and the improved differential evolution algorithm used to solve the problem is presented in Section 5. Next, numerical simulations and analysis are presented in Section 6. The conclusions are given in Section 7.

2. Relative motion dynamics model

As shown in Fig. 1, the cylindrical coordinates are defined as follows. Firstly, a fixed reference plane coincides with the initial orbit plane of the chief satellite (Chief) can be established, where the normal vector to this plane can be denoted by the unit vectors $\boldsymbol{i}_z$. The components on the reference plane will be represented by unit vectors of two polar coordinates $\boldsymbol{i}_{\rho_c}$ and $\boldsymbol{i}_{\theta_c}$. Then, the Chief's motion space can be described by a set of cylindrical coordinates ρ_c, θ_c, and z_c. The position of the Chief includes in-plane and out-of-plane parts as follows:

$$\boldsymbol{r}_c = \rho_c \boldsymbol{i}_{\rho_c} + z_c \boldsymbol{i}_z. \tag{1}$$

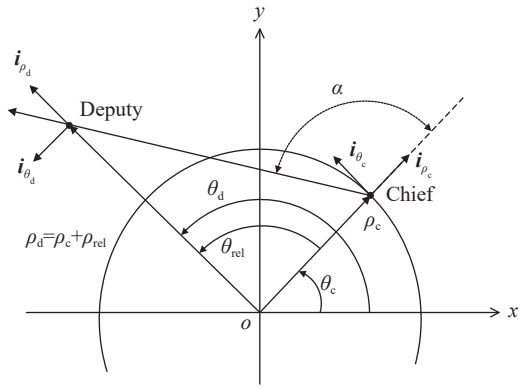

Fig. 1 Cylindrical coordinates in x-y plane [48]

The first and second derivatives of the position with respect to time are governed by

$$\begin{cases} \boldsymbol{v}_c = \dot{\rho}_c \boldsymbol{i}_{\rho_c} + \rho_c \dot{\theta}_c \boldsymbol{i}_{\theta_c} + \dot{z}_c \boldsymbol{i}_z \\ \boldsymbol{a}_c = \left(\ddot{\rho}_c - \rho_c \dot{\theta}_c^2\right) \boldsymbol{i}_{\rho_c} + \left(\rho_c \ddot{\theta}_c + 2\dot{\rho}_c \dot{\theta}_c\right) \boldsymbol{i}_{\theta_c} + \ddot{z}_c \boldsymbol{i}_z \end{cases}. \tag{2}$$

Meanwhile, the orbital motion of the spacecraft in two-body environment without considering other perturbations can be given as follows:

$$\boldsymbol{a}_c = -\frac{\mu}{r_c^3} \boldsymbol{r}_c. \tag{3}$$

Then, the orbit dynamics for the Chief in cylindrical coordinates are obtained by equating the components of (3) to (1). Similarly, the motion of the deputy satellite (Deputy) also can be modeled in cylindrical coordinates. After that, the parameterized relative motion states under cylindrical system can be defined as

$$\begin{cases} \rho_{rel} = \rho_d - \rho_c \\ \theta_{rel} = \theta_d - \theta_c \\ z_{rel} = z_d - z_c \end{cases} \tag{4}$$

where the subscript d stands for Deputy.

Then, under the assumptions that the relative range is much smaller than the orbital radius of the satellite and relative orbit rate is far smaller than the orbit rate, a Clohessy-Wiltshire look like model can be obtained in cylindrical coordinates by the expansion to first-order in Taylor series [50] as follows:

$$\begin{cases} \ddot{\rho}_{rel} \approx 3n^2 \rho_{rel} + 2Rn\dot{\theta}_{rel} \\ \ddot{\theta}_{rel} \approx -\dfrac{2n}{R}\dot{\rho}_{rel} \\ \ddot{z}_{rel} \approx -n^2 z_{rel} \end{cases} \tag{5}$$

where n is the orbital rate of the chief satellite, and R is the orbital radius of the chief satellite.

Let the relative orbital motion state in cylindrical coordinates be the "position" and "velocity" as

$$\boldsymbol{X} = \begin{bmatrix} \rho_{rel} & \theta_{rel} & z_{rel} & \dot{\rho}_{rel} & \dot{\theta}_{rel} & \dot{z}_{rel} \end{bmatrix}^{\mathrm{T}}. \tag{6}$$

Then, the relative motion dynamics model in cylindrical coordinates can be solved analytically and the following state transition form can be obtained

$$\boldsymbol{X}(t) = \boldsymbol{\Phi}(t) \boldsymbol{X}_0 \tag{7}$$

where $\boldsymbol{\Phi}(t)$ is the state transition matrix and $\boldsymbol{X}_0$ denotes the initial relative state. The expression for $\boldsymbol{\Phi}(t)$ is as follows:

$$\boldsymbol{\Phi}(t) = \begin{bmatrix} 4-3\cos(nt) & 0 & 0 & \dfrac{\sin(nt)}{n} & \dfrac{2R}{n}[1-\cos(nt)] & 0 \\ \dfrac{6[\sin(nt)-nt]}{R} & 1 & 0 & \dfrac{2[\cos(nt)-1]}{nR} & \dfrac{4\sin(nt)-3nt}{n} & 0 \\ 0 & 0 & \cos(nt) & 0 & 0 & \dfrac{\sin(nt)}{n} \\ 3n\sin(nt) & 0 & 0 & \cos(nt) & 2R\sin(nt) & 0 \\ \dfrac{6n[\cos(nt)-1]}{R} & 0 & 0 & \dfrac{-2\sin(nt)}{R} & 4\cos(nt)-3 & 0 \\ 0 & 0 & -n\sin(nt) & 0 & 0 & \cos(nt) \end{bmatrix}. \tag{8}$$

Each row from top to bottom in the state transition matrix shown in (8) can be represented by the corresponding partitions $\boldsymbol{\Phi}_\rho(t)$, $\boldsymbol{\Phi}_\theta(t)$, $\boldsymbol{\Phi}_z(t)$, $\boldsymbol{\Phi}_{\dot\rho}(t)$, $\boldsymbol{\Phi}_{\dot\theta}(t)$, and $\boldsymbol{\Phi}_{\dot z}(t)$, respectively, which is the state transition matrix corresponding to each component of the relative state.

3. Measurement equation

The LOS measurement geometry in cylindrical coordinates is shown in Fig. 2.

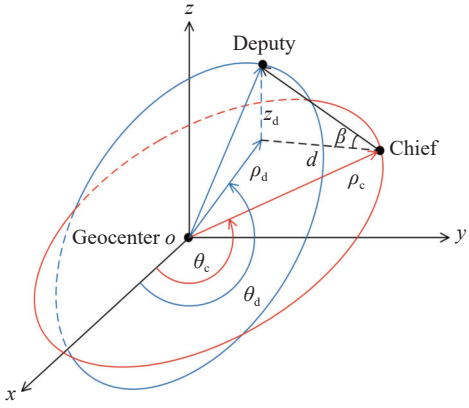

Fig. 2 Geometry in cylindrical coordinates

Combining Fig. 1 and Fig. 2, the relationship between two LOS angles and the relative states is modeled as

$$\begin{cases} \tan\alpha = \dfrac{(\rho_c+\rho_{rel})\sin\theta_{rel}}{(\rho_c+\rho_{rel})\cos\theta_{rel}-\rho_c} = \\ \qquad \dfrac{\sin\theta_{rel}}{\left[\cos\theta_{rel}-\dfrac{\rho_c}{\rho_c+\rho_{rel}}\right]} \\ \tan\beta = \dfrac{z_{rel}}{d} \end{cases} \tag{9}$$

where d is the distance projected by the chief satellite and the deputy satellite on the orbital plane of the chief satellite, which can be calculated as

$$d = \sqrt{\rho_d^2+\rho_c^2-2\rho_c\rho_d\cos\theta_{rel}}. \tag{10}$$

Under the assumption that the LOS angles measurements are disturbed by zero mean Gaussian white noises, the measurement is governed by

$$z = \begin{bmatrix} \alpha+v_\theta \\ \beta+w_\theta \end{bmatrix} = \begin{bmatrix} \arctan\left(\dfrac{\sin\theta_{rel}}{\cos\theta_{rel}-\dfrac{\rho_c}{\rho_c+\rho_{rel}}}\right)+v_\theta \\ \arctan\left(\dfrac{z_{rel}}{d}\right)+w_\theta \end{bmatrix} \tag{11}$$

where v_θ and w_θ are the noises.

4. Observability analysis

The observability problem is to check whether or not the initial relative orbit can be uniquely determined from LOS measurements. Then, the observability analysis can be conducted as follows.

According to the definition, the relative position vector in the inertial coordinates is as follows:

$$\boldsymbol{r}_d-\boldsymbol{r}_c = \rho_d\boldsymbol{i}_{\rho_d}+z_d\boldsymbol{i}_{z_d}-(\rho_c\boldsymbol{i}_{\rho_c}+z_c\boldsymbol{i}_{z_c}). \tag{12}$$

Because the angle between the vectors $\boldsymbol{i}_{\rho_d}$ and $\boldsymbol{i}_{\rho_c}$ is θ_{rel}, $\boldsymbol{i}_{\rho_d}$ can be calculated from $\boldsymbol{i}_{\rho_c}$ and $\boldsymbol{i}_{\theta_c}$:

$$\boldsymbol{i}_{\rho_d} = \cos\theta_{rel}\boldsymbol{i}_{\rho_c}+\sin\theta_{rel}\boldsymbol{i}_{\theta_c}. \tag{13}$$

Substituting (13) and the equation $\boldsymbol{i}_{z_d}=\boldsymbol{i}_{z_c}$ into (12) produces

$$\boldsymbol{r}_d-\boldsymbol{r}_c = (\rho_d\cos\theta_{rel}-\rho_c)\boldsymbol{i}_{\rho_c}+\rho_d\sin\theta_{rel}\boldsymbol{i}_{\theta_c}+z_{rel}\boldsymbol{i}_{z_c}. \tag{14}$$

Substituting (4) into (14) and unitizing yields the LOS vector:

$$\boldsymbol{i}_{los} = \frac{\boldsymbol{r}_d-\boldsymbol{r}_c}{\|\boldsymbol{r}_d-\boldsymbol{r}_c\|} = \frac{((\rho_{rel}+\rho_c)\cos\theta_{rel}-\rho_c)\boldsymbol{i}_{\rho_c}+(\rho_{rel}+\rho_c)\sin\theta_{rel}\boldsymbol{i}_{\theta_c}+z_{rel}\boldsymbol{i}_{z_c}}{\sqrt{\rho_{rel}^2+2\rho_c^2+z_{rel}^2+2\rho_c\rho_{rel}-2\rho_c(\rho_{rel}+\rho_c)\cos\theta_{rel}}}. \tag{15}$$

Then, the LOS measurement profile observed for any initial relative state $\boldsymbol{X}_0=[\rho_{rel0},\theta_{rel0},z_{rel0},\dot\rho_{rel0},\dot\theta_{rel0},\dot z_{rel0}]^{\mathrm{T}}$ can be obtained by substituting (7) into (15) as follows:

$$\boldsymbol{i}_{los}(t) = \frac{((\boldsymbol{\Phi}_\rho(t)\boldsymbol{X}_0+\rho_c)\cos(\boldsymbol{\Phi}_\theta(t)\boldsymbol{X}_0)-\rho_c)\boldsymbol{i}_{\rho_c}+(\boldsymbol{\Phi}_\rho(t)\boldsymbol{X}_0+\rho_c)\sin(\boldsymbol{\Phi}_\theta(t)\boldsymbol{X}_0)\boldsymbol{i}_{\theta_c}+\boldsymbol{\Phi}_z(t)\boldsymbol{X}_0\boldsymbol{i}_{z_c}}{\sqrt{(\boldsymbol{\Phi}_\rho(t)\boldsymbol{X}_0)^2+2\rho_c^2+(\boldsymbol{\Phi}_z(t)\boldsymbol{X}_0)^2+2\rho_c\boldsymbol{\Phi}_\rho(t)\boldsymbol{X}_0-2\rho_c(\boldsymbol{\Phi}_\rho(t)\boldsymbol{X}_0+\rho_c)\cos(\boldsymbol{\Phi}_\theta(t)\boldsymbol{X}_0)}}. \tag{16}$$

Next, the observed LOS profile of scaled initial relative state $k\boldsymbol{X}_0$ by any factor $k>0$ can be govern as follows:

$$\boldsymbol{i}_{los}(t) = \frac{((k\boldsymbol{\Phi}_\rho(t)\boldsymbol{X}_0+\rho_c)\cos(k\boldsymbol{\Phi}_\theta(t)\boldsymbol{X}_0)-\rho_c)\boldsymbol{i}_{\rho_c}+(k\boldsymbol{\Phi}_\rho(t)\boldsymbol{X}_0+\rho_c)\sin(k\boldsymbol{\Phi}_\theta(t)\boldsymbol{X}_0)\boldsymbol{i}_{\theta_c}+k\boldsymbol{\Phi}_z(t)\boldsymbol{X}_0\boldsymbol{i}_{z_c}}{\sqrt{(k\boldsymbol{\Phi}_\rho(t)\boldsymbol{X}_0)^2+2\rho_c^2+(k\boldsymbol{\Phi}_z(t)\boldsymbol{X}_0)^2+2k\rho_c\boldsymbol{\Phi}_\rho(t)\boldsymbol{X}_0-2\rho_c(k\boldsymbol{\Phi}_\rho(t)\boldsymbol{X}_0+\rho_c)\cos(k\boldsymbol{\Phi}_\theta(t)\boldsymbol{X}_0)}}. \tag{17}$$

Obviously, the model for LOS vector in cylindrical coordinates is strongly nonlinear which contains trigonometric function. It can be seem that the scale factor k in the numerator and denominator cannot be eliminated without conditions. As we know, if the scale factor can be eliminated, different relative orbits share the same LOS

vector profile, which means unobservable. When the relative phase angle $\theta_{\text{rel}} = \boldsymbol{\Phi}_\theta \boldsymbol{X}_0 = 0$, (17) is reduced to the following form:

$$\boldsymbol{i}_{\text{los}} = \frac{\boldsymbol{\Phi}_\rho(t)\boldsymbol{X}_0\boldsymbol{i}_{\rho_c} + \boldsymbol{\Phi}_z(t)\boldsymbol{X}_0\boldsymbol{i}_{z_c}}{\sqrt{(\boldsymbol{\Phi}_\rho(t)\boldsymbol{X}_0)^2 + (\boldsymbol{\Phi}_z(t)\boldsymbol{X}_0)^2}} = \frac{k\boldsymbol{\Phi}_\rho(t)\boldsymbol{X}_0\boldsymbol{i}_{\rho_c} + k\boldsymbol{\Phi}_z(t)\boldsymbol{X}_0\boldsymbol{i}_{z_c}}{\sqrt{(k\boldsymbol{\Phi}_\rho(t)\boldsymbol{X}_0)^2 + (k\boldsymbol{\Phi}_z(t)\boldsymbol{X}_0)^2}}. \tag{18}$$

Apparently, the state is unobservable in this case because the LOS profiles are not unique to a given set of initial relative states. However, the phase angle would not be zero all the time during the flight except the case of co-orbit with different phases. Thus, the angles-only system established in cylindrical coordinates is generally observable. Anyway, there may be other unobservable cases, but because of the strong nonlinearity of the measurement model, the number of the unobservable cases would be very limited.

5. Initial relative orbit determination frame

Initial relative orbit determination (IROD) is a process that the LOS angles during a set of orbital arc are measured and processed to fit a six dimensional solution for the initial relative orbit. This process is a data regression problem, which can be realized by establishing an objective function and finding the optimal solution to minimize (or maximize) the value of the objective function. For linear systems, the least square method can be used for data regression, whilst intelligent optimization algorithms are commonly required for regression problems of nonlinear systems. The relative orbit dynamics model and LOS angle measurement model in cylindrical system adopted in this paper have strong nonlinearity, so the regression fitting is very difficult. The ordinary optimization algorithm is very easy to fall into the local optimal solution. However, differential evolution (DE) is a relatively new optimization method, which is simple, fast, and robust, and has great advantages in solving nonlinear problems [52]. Therefore, this paper designs an angles-only relative orbit determination algorithm based on differential evolution algorithm in cylindrical system. Now, the problem is to construct the angles-only IROD frame by using the DE algorithm, which is presented in the following.

Firstly, the measurement model shown in (9) can be transformed into the following form:

$$\begin{cases} \left(\cos\theta_{\text{rel}} - \dfrac{\rho_c}{\rho_c + \rho_{\text{rel}}}\right)\tan\alpha - \sin\theta_{\text{rel}} = 0 \\ \sqrt{(\rho_c + \rho_{\text{rel}})^2 + \rho_c^2 - 2\rho_c(\rho_c + \rho_{\text{rel}})\cos\theta_{\text{rel}}}\tan\beta - z_{\text{rel}} = 0 \end{cases}. \tag{19}$$

Then, the state components ρ_{rel}, θ_{rel}, and z_{rel} in (19) can be given in the form of state transition of the initial relative orbital state $\boldsymbol{X}_0$, namely $\boldsymbol{\Phi}_\rho(t)\boldsymbol{X}_0$, $\boldsymbol{\Phi}_\theta(t)\boldsymbol{X}_0$, $\boldsymbol{\Phi}_z(t)\boldsymbol{X}_0$, and a nonlinear system of equations with unknown variable $\boldsymbol{X}_0$ can be obtained after substitution.

$$\begin{cases} \left(\cos[\boldsymbol{\Phi}_\theta(t)\boldsymbol{X}_0] - \dfrac{\rho_c}{\rho_c + \boldsymbol{\Phi}_\rho(t)\boldsymbol{X}_0}\right)\tan\alpha - \sin[\boldsymbol{\Phi}_\theta(t)\boldsymbol{X}_0] = 0 \\ \sqrt{(\rho_c + \boldsymbol{\Phi}_\rho(t)\boldsymbol{X}_0)^2 + \rho_c^2 - 2\rho_c(\rho_c + \boldsymbol{\Phi}_\rho(t)\boldsymbol{X}_0)\cos[\boldsymbol{\Phi}_\theta(t)\boldsymbol{X}_0]}\tan\beta - \boldsymbol{\Phi}_z(t)\boldsymbol{X}_0 = 0 \end{cases} \tag{20}$$

Equation (20) contains two scalar equations, but the corresponding quantity $\boldsymbol{X}_0$ is six-dimensional. Obviously, in the case of only one set of LOS angle measurements, no unique solution can be obtained. Obviously, it requires at least three sets of LOS angle measurements to obtain six equations to solve the problem. When $n \geq 3$ sets of LOS angles are available,

$$\begin{cases} \left(\cos[\boldsymbol{\Phi}_\theta(t_1)\boldsymbol{X}_0] - 1 + \dfrac{\boldsymbol{\Phi}_\rho(t_1)\boldsymbol{X}_0}{\rho_c + \boldsymbol{\Phi}_\rho(t_1)\boldsymbol{X}_0}\right)\tan\alpha_1 - \sin[\boldsymbol{\Phi}_\theta(t_1)\boldsymbol{X}_0] = 0 \\ \sqrt{(\rho_c + \boldsymbol{\Phi}_\rho(t_1)\boldsymbol{X}_0)^2 + \rho_c^2 - 2\rho_c(\rho_c + \boldsymbol{\Phi}_\rho(t_1)\boldsymbol{X}_0)\cos[\boldsymbol{\Phi}_\theta(t_1)\boldsymbol{X}_0]}\tan\beta_1 - \boldsymbol{\Phi}_z(t_1)\boldsymbol{X}_0 = 0 \\ \left(\cos[\boldsymbol{\Phi}_\theta(t_2)\boldsymbol{X}_0] - 1 + \dfrac{\boldsymbol{\Phi}_\rho(t_2)\boldsymbol{X}_0}{\rho_c + \boldsymbol{\Phi}_\rho(t_2)\boldsymbol{X}_0}\right)\tan\alpha_2 - \sin[\boldsymbol{\Phi}_\theta(t_2)\boldsymbol{X}_0] = 0 \\ \sqrt{(\rho_c + \boldsymbol{\Phi}_\rho(t_2)\boldsymbol{X}_0)^2 + \rho_c^2 - 2\rho_c(\rho_c + \boldsymbol{\Phi}_\rho(t_2)\boldsymbol{X}_0)\cos[\boldsymbol{\Phi}_\theta(t_2)\boldsymbol{X}_0]}\tan\beta_2 - \boldsymbol{\Phi}_z(t_2)\boldsymbol{X}_0 = 0 \\ \vdots \\ \left(\cos[\boldsymbol{\Phi}_\theta(t_n)\boldsymbol{X}_0] - 1 + \dfrac{\boldsymbol{\Phi}_\rho(t_n)\boldsymbol{X}_0}{\rho_c + \boldsymbol{\Phi}_\rho(t_n)\boldsymbol{X}_0}\right)\tan\alpha_n - \sin[\boldsymbol{\Phi}_\theta(t_n)\boldsymbol{X}_0] = 0 \\ \sqrt{(\rho_c + \boldsymbol{\Phi}_\rho(t_n)\boldsymbol{X}_0)^2 + \rho_c^2 - 2\rho_c(\rho_c + \boldsymbol{\Phi}_\rho(t_n)\boldsymbol{X}_0)\cos[\boldsymbol{\Phi}_\theta(t_n)\boldsymbol{X}_0]}\tan\beta_n - \boldsymbol{\Phi}_z(t_n)\boldsymbol{X}_0 = 0 \end{cases}. \tag{21}$$

Equation (21) is a nonlinear system of equations with unknown quantity $\boldsymbol{X}_0$, so it is difficult to find an analytical solution directly that an optimal solution can be obtained through fitting to make it closer to the physical solution. In this paper, DE optimization is introduced to solve the above nonlinear equations.

The first thing to do is to construct the optimal index. Assuming that the fitting solution is $\hat{\boldsymbol{X}}_0$, the result obtained by substituting $\hat{\boldsymbol{X}}_0$ into the left-hand side of the equation set shown in (21) should be as close to 0 as possible. Therefore, the parameter $\boldsymbol{L}$ is defined as follows:

$$\boldsymbol{L}=\begin{bmatrix}\dfrac{\left(\cos[\boldsymbol{\Phi}_\theta(t_1)\hat{\boldsymbol{X}}_0]-1+\dfrac{\boldsymbol{\Phi}_\rho(t_1)\hat{\boldsymbol{X}}_0}{\rho_{\mathrm{c}}+\boldsymbol{\Phi}_\rho(t_1)\hat{\boldsymbol{X}}_0}\right)\tan\alpha_1-\sin[\boldsymbol{\Phi}_\theta(t_1)\hat{\boldsymbol{X}}_0]}{\sqrt{(\rho_{\mathrm{c}}+\boldsymbol{\Phi}_\rho(t_1)\hat{\boldsymbol{X}}_0)^2+\rho_{\mathrm{c}}^2-2\rho_{\mathrm{c}}(\rho_{\mathrm{c}}+\boldsymbol{\Phi}_\rho(t_1)\hat{\boldsymbol{X}}_0)\cos[\boldsymbol{\Phi}_\theta(t_1)\hat{\boldsymbol{X}}_0]}\tan\beta_1-\boldsymbol{\Phi}_z(t_1)\hat{\boldsymbol{X}}_0}\\ \dfrac{\left(\cos[\boldsymbol{\Phi}_\theta(t_2)\hat{\boldsymbol{X}}_0]-1+\dfrac{\boldsymbol{\Phi}_\rho(t_2)\hat{\boldsymbol{X}}_0}{\rho_{\mathrm{c}}+\boldsymbol{\Phi}_\rho(t_2)\hat{\boldsymbol{X}}_0}\right)\tan\alpha_2-\sin[\boldsymbol{\Phi}_\theta(t_2)\hat{\boldsymbol{X}}_0]}{\sqrt{(\rho_{\mathrm{c}}+\boldsymbol{\Phi}_\rho(t_2)\hat{\boldsymbol{X}}_0)^2+\rho_{\mathrm{c}}^2-2\rho_{\mathrm{c}}(\rho_{\mathrm{c}}+\boldsymbol{\Phi}_\rho(t_2)\hat{\boldsymbol{X}}_0)\cos[\boldsymbol{\Phi}_\theta(t_2)\hat{\boldsymbol{X}}_0]}\tan\beta_2-\boldsymbol{\Phi}_z(t_2)\hat{\boldsymbol{X}}_0}\\ \vdots\\ \dfrac{\left(\cos[\boldsymbol{\Phi}_\theta(t_n)\hat{\boldsymbol{X}}_0]-1+\dfrac{\boldsymbol{\Phi}_\rho(t_n)\hat{\boldsymbol{X}}_0}{\rho_{\mathrm{c}}+\boldsymbol{\Phi}_\rho(t_n)\hat{\boldsymbol{X}}_0}\right)\tan\alpha_n-\sin[\boldsymbol{\Phi}_\theta(t_n)\hat{\boldsymbol{X}}_0]}{\sqrt{(\rho_{\mathrm{c}}+\boldsymbol{\Phi}_\rho(t_n)\hat{\boldsymbol{X}}_0)^2+\rho_{\mathrm{c}}^2-2\rho_{\mathrm{c}}(\rho_{\mathrm{c}}+\boldsymbol{\Phi}_\rho(t_n)\hat{\boldsymbol{X}}_0)\cos[\boldsymbol{\Phi}_\theta(t_n)\hat{\boldsymbol{X}}_0]}\tan\beta_n-\boldsymbol{\Phi}_z(t_n)\hat{\boldsymbol{X}}_0}\end{bmatrix}. \tag{22}$$

The closer the vector $\boldsymbol{L}$ approaches the zero vector, the closer $\hat{\boldsymbol{X}}_0$ approaches the physical solution. Considering that the modulus length index is very suitable for measuring whether a vector is approaching zero, here we define a function $f=\boldsymbol{L}^{\mathrm{T}}\boldsymbol{L}$ (i.e., the square of the modulus length of the vector $\boldsymbol{L}$), so that $\hat{\boldsymbol{X}}_0$ with the minimum value of f is the optimal solution. Therefore, the optimization function is defined as

$$\min f=\boldsymbol{L}^{\mathrm{T}}\boldsymbol{L}. \tag{23}$$

6. Improved DE algorithm

DE algorithm is a random optimization method based on population [52,53]. Different from the genetic algorithm, the mutation operator of DE algorithm is obtained by the difference between multiple pairs of vectors arbitrarily selected in the population, which could perform better on nonlinear problems than genetic algorithms. In recent years, DE algorithm has been applied successfully in many fields [54,55]. Generally, DE algorithms are mainly divided into four steps: population initialization, mutation, crossover, and selection. Steps for the proposed improved DE algorithm are presented in detail as follows.

6.1 Initialization

The population size (the total number of individuals in each generation) is initialized as N_P, the solution space dimension of the target is D, the initial population is $\boldsymbol{X}^0$, and the population that has evolved to the tth generation is $\boldsymbol{X}^t$. The ith individual in the initial population is $\boldsymbol{x}_i^0$, and the jth component of the ith individual is $x_{i,j}$.

$$\boldsymbol{X}^0=\left[x_1^0,x_2^0,\cdots,x_{N_{\mathrm{p}}}^0\right], \tag{24}$$

$$\boldsymbol{X}^t=\left[x_1^t,x_2^t,\cdots,x_{N_{\mathrm{p}}}^t\right], \tag{25}$$

$$\boldsymbol{x}_i^0=\left[x_{i,1}^0,x_{i,2}^0\ \cdots,x_{i,D}^0\right], \tag{26}$$

$$x_{i,j}=x_{j,\min}+\mathrm{rand}(x_{j,\max}-x_{j,\min}), \tag{27}$$

where $x_{j,\max}$ is the upper bound of the jth component of the feasible solution space of the target being searched, $x_{j,\min}$ is the lower bound of the jth component of the feasible solution space, and rand$(\cdot)$ is a random function used to generate a random number between 0 and 1.

6.2 Mutation

For the ith individual x_i^t in the tth generation population, the mutation vector $\boldsymbol{V}_i^{t+1}$ generated by DE can be composed of D components v_i^{t+1}:

$$\boldsymbol{V}_i^{t+1}=\left[v_{i,1}^{t+1},v_{i,2}^{t+1},\cdots,v_{i,D}^{t+1}\right], \tag{28}$$

$$v_{i,j}^{t+1}=x_{i,j}^t+F\left(x_{\mathrm{best},j}^t-x_{i,j}^t\right)+F\left(x_{r_1,j}^t-x_{r_2,j}^t\right), \tag{29}$$

where $i=1,2,\cdots,N_P$, $j=1,2,\cdots,D$, x_{best}^t is the optimal individual in the population of the tth generation, and $x_{r_1}^t,x_{r_2}^t$ respectively are the two individuals randomly selected in the population of the tth generation after excluding the ith individual x_i^t and the optimal individual x_{best}^t. The optimal individual x_{best}^t of each generation will not conduct mutation, crossover and other operations, and

will be completely retained to the next generation. F is the scaling factor ($0 \leqslant F \leqslant 2$), which is used to control the influence of difference quantity $x_{r_2,j}^t - x_{r_3,j}^t$ on the mutation quantity. When F is large, it is efficient and fast in global search, which is suitable for optimization in the early stage; however, in the later stage of optimization, a large scaling factor will not be conducive to the local search of the algorithm [55]. Therefore, the scaling factor designed in this paper is in decreasing form:

$$F^t = F^1 - \left(F^1 - 0.5\right)\frac{t}{N_P} \tag{30}$$

where F^t is the tth generation scaling factor, with $F^1 = 0.9$.

6.3 Crossover

The ith individual x_i^t in the tth generation population is randomly recombined with each component of its mutation vector $\boldsymbol{V}_i^{t+1}$, and the new vector obtained after recombination is $\boldsymbol{u}_i^{t+1}$, i.e., the crossover vector:

$$\boldsymbol{u}_i^{t+1} = \left[u_{i,1}^{t+1}, u_{i,2}^{t+1}, \cdots, u_{i,D}^{t+1}\right], \tag{31}$$

$$u_{i,j}^{t+1} = \begin{cases} v_{i,j}^{t+1} & b \leqslant c_R \text{ or } j = r \\ x_{i,j}^t & b > c_R \text{ or } j \neq r \end{cases}, \tag{32}$$

where $i = 1, 2, \cdots, N_P$, $j = 1, 2, \cdots, D$, and b is a random number between 0 and 1. c_R is a crossover factor, which is a real number between 0 and 1. r is called the crossover probability, which is an integer randomly selected from 0 to D. When c_R is small, the local search efficiency of the algorithm is high, which is suitable for the early optimization stage. In the later stage of optimization, a larger c_R can prevent the algorithm from falling into local optimization, so the crossover factor adopted in this paper is also dynamic:

$$c_R^t = c_R^1 + \left(0.6 - c_R^1\right)\frac{t}{N_P} \tag{33}$$

where c_R^t is the crossover factor of the tth generation, and $c_R^1 = 0.3$.

6.4 Selection

As shown in (14), the ith individual in the $(t+1)$th generation population generated by the optimization function is $\boldsymbol{x}_i^{t+1}$, and the jth component of the ith individual is $x_{i,j}^{t+1}$. The specific selection process is as follows:

$$x_{i,j}^{t+1} = \begin{cases} u_{i,j}^{t+1}, & f\left(u_{i,j}^{t+1}\right) < f\left(x_{i,j}^t\right) \\ x_{i,j}^t, & f\left(u_{i,j}^{t+1}\right) \geqslant f\left(x_{i,j}^t\right) \end{cases} \tag{34}$$

where $f(\cdot)$ denotes the optimization function as shown in (23).

7. Numerical simulation and analysis

In this section, two different types of application are considered to demonstrate the validity of the proposed algorithm, i.e., geosynchronous Earth orbit (GEO) and low Earth orbit (LEO). The orbit parameters for the simulation cases will be presented in the following subsections. The population size for DE algorithm is chosen to be 100 while the total genetic generation is limited to 500. The number of the pair of LOS angles is set to be 30 and the medium level of the camera accuracy is assumed to be available onboard that the standard deviation of angle measurement noise is set to be 0.005°.

The IROD performance index for evaluating the algorithm will be introduced first in the rest of this section while the simulation results with analysis will be presented next.

7.1 Performance index

Since the observability of relative orbit states without distance measurements is the most important problem to be solved in angles-only orbit determination, the most direct and essential index of relative orbit determination performance is the estimation error of relative distance. At the same time, because the performance of the angles-only orbit determination has a certain relationship with the distance between the two spacecraft to some extent, the ratio of relative distance estimation error and real distance will be used as the orbit determination performance index in the subsequent simulation analysis.

However, it is difficult to convert relative orbit states into relative distance information directly under cylindrical system, so the near-focus coordinate system can be introduced for transfer. The cylindrical system coordinates of the chief and the deputy satellites can be converted to the near-focus coordinate system:

$$\begin{cases} x_{\mathrm{c}} = \rho_{\mathrm{c}}\cos\theta_{\mathrm{c}} \\ y_{\mathrm{c}} = \rho_{\mathrm{c}}\sin\theta_{\mathrm{c}} \\ z_{\mathrm{c}} = z_{\mathrm{c}} \end{cases}, \tag{35}$$

$$\begin{cases} x_{\mathrm{d}} = \rho_{\mathrm{d}}\cos\theta_{\mathrm{d}} = (\rho_{\mathrm{c}} + \rho_{\mathrm{rel}})\cos(\theta_{\mathrm{c}} + \theta_{\mathrm{rel}}) \\ y_{\mathrm{d}} = \rho_{\mathrm{d}}\sin\theta_{\mathrm{d}} = (\rho_{\mathrm{c}} + \rho_{\mathrm{rel}})\sin(\theta_{\mathrm{c}} + \theta_{\mathrm{rel}}) \\ z_{\mathrm{d}} = z_{\mathrm{c}} + z_{\mathrm{rel}} \end{cases}. \tag{36}$$

Then the actual distance l between the Chief and Deputy satellites is calculated as follows:

$$l = \sqrt{(x_{\mathrm{d}} - x_{\mathrm{c}})^2 + (y_{\mathrm{d}} - y_{\mathrm{c}})^2 + (z_{\mathrm{d}} - z_{\mathrm{c}})^2}. \tag{37}$$

When the estimation errors are considered, (36) becomes the following form:

$$\begin{cases} x_d' = \rho_d'\cos\theta_d' = (\rho_{\mathrm{c}} + \rho_{\mathrm{rel}} + \delta\rho)\cos(\theta_{\mathrm{c}} + \theta_{\mathrm{rel}} + \delta\theta) \\ y_d' = \rho_d'\sin\theta_d' = (\rho_{\mathrm{c}} + \rho_{\mathrm{rel}} + \delta\rho)\sin(\theta_{\mathrm{c}} + \theta_{\mathrm{rel}} + \delta\theta) \\ z_d' = z_{\mathrm{c}} + z_{\mathrm{rel}} + \delta z \end{cases} \tag{38}$$

where $\delta\rho$, $\delta\theta$, and δz represent the estimate errors in cylindrical coordinate system.

In order to better characterize error characteristics, the percentage error is defined as the ratio of distance estimation error e to relative distance, i.e.,

$$e_p = \frac{\sqrt{(x'_{\rm d}-x_{\rm d})^2+(y'_{\rm d}-y_{\rm d})^2+(z'_{\rm d}-z_{\rm d})^2}}{\sqrt{(x_{\rm d}-x_{\rm c})^2+(y_{\rm d}-y_{\rm c})^2+(z_{\rm d}-z_{\rm c})^2}}\times 100\%. \quad (39)$$

The subsequent simulation analysis will be carried out based on this error parameter.

7.2 GEO cases

It is assumed that the Chief is orbiting in GEO area while the Deputy's orbit is 100−200 km higher than that of the Chief and with a small eccentricity and inclination with respect to Chief. Orbit parameters are shown in Table 1. The relative distance at the initial epoch is about 1 000−2 000 km. Moreover, the total measurement span is set to be 14 400 s. It should be noted that the Chief and Deputy are almost orbiting in co-planar circular orbits, thus it is quite different to capture the nonlinearity for angles-only problem. As a result, a relative long measurement span is required. In addition, the guess for the feasible solution search space is shown in Table 2, where α is one of the angle information measured by the camera at the initial moment.

Table 1 Parameters setting of Chief and Deputy

Orbital element	Chief	Deputy		
		Case 1	Case 2	Case 3
Semimajor axis/km	42 164.17	42 264.17	42 264.17	42 364.17
Eccentricity	0	0.000 1	0.000 1	0.000 1
Inclination/(°)	0	0.000 02	0.000 02	0.000 02
Right ascension of ascending node/(°)	0	0	0	0
Argument of perigee/(°)	0	0	0	0
True anomaly/(°)	322.764 5	324.115 1	325.46	324.093

Table 2 Setting of feasible solution space guess

State	Minimum	Maximum
$\rho_{\rm rel}$/m	100 000	3 000 000
$\theta_{\rm rel}$/rad	0	0. 1α
$z_{\rm rel}$/m	−2 000	2 000
$\dot{\rho}_{\rm rel}$/(m/s)	−2	2
$\dot{\theta}_{\rm rel}$/(rad/s)	−0.000 01α	0.000 01α
$\dot{z}_{\rm rel}$/(m/s)	−20	20

The convergence curves of the optimization function for the three cases are shown in Fig. 3. Sel_best in the table during optimization is the optimization function value corresponding to the optimal individual.

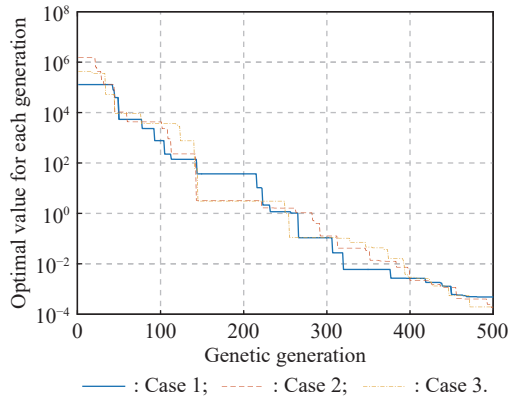

Fig. 3 Convergence curves of optimization function

The simulation results are shown in Table 3 to Table 5, where the optimal IROD solution and percentage errors from four runs of the simulation are with same parameters.

Table 3 Optimization results for Case 1

State	Run #1	Run #2	Run #3	Run #4
Sel_best	0.000 482	0.003 928	0.001 034	0.000 814
$\rho_{\rm rel}$/m	99 342.4	183 869.0	175 715.5	130 469.7
$\theta_{\rm rel}$/rad	0.023 193	0.040 047	0.038 522	0.029 747
$z_{\rm rel}$/m	0.007 945	0.007 754	−0.059 337	−0.016 427
$\dot{\rho}_{\rm rel}$/(m/s)	−0.530 838	−1.018 791	−0.876 775	−0.525 139
$\dot{\theta}_{\rm rel}$/(rad/s)	−2.483 7 e−07	−4.605 3 e−07	−4.391 6 e−07	−3.285 6 e−07
$\dot{z}_{\rm rel}$/(m/s)	−3.743 0 e-06	4.148 0 e−06	1.547 0 e−05	5.170 7 e−06
Error/%	1.601 9	70.198 5	63.692 7	26.284 3

Table 4 Optimization results for Case 2

State	Run #1	Run #2	Run #3	Run #4
Sel_best	0.000 297	0.000 149	0.000 193	0.000 132
$\rho_{\rm rel}$/m	129 523.9	108 668.7	128 224.8	120 088.4
$\theta_{\rm rel}$/rad	0.055 997	0.049 735	0.055 685	0.053 446
$z_{\rm rel}$/m	−0.041 245	0.008 858	−0.022 159	0.006 543
$\dot{\rho}_{\rm rel}$/(m/s)	−0.109 385	−0.368 671	−0.230 537	0.241 181
$\dot{\theta}_{\rm rel}$/(rad/s)	−3.455 5 e−07	−2.744 5 e−07	−3.313 3 e−07	−3.302 6 e−07
$\dot{z}_{\rm rel}$/(m/s)	5.887 4 e−06	−1.634 8 e−05	1.297 9 e−05	−1.354 8 e−05
Error/%	19.094 6	5.736 2	18.428 9	13.648 9

Table 5 Optimization results for Case 3

State	Run #1	Run #2	Run #3	Run #4
Sel_best	0.000 154	0.000 251	0.000 062	0.000 290
$\rho_{\rm rel}$/m	238 250.4	187 168.5	200 431.8	212 928.5
$\theta_{\rm rel}$/rad	0.021 730	0.020 696	0.023 536	0.024 695
$z_{\rm rel}$/m	0.004 079	0.020 357	−0.012 792	−0.022 222
$\dot{\rho}_{\rm rel}$/(m/s)	−0.816 903	−0.321 888	−0.570 304	0.201 456
$\dot{\theta}_{\rm rel}$/(rad/s)	−6.953 6 e−07	−4.822 3 e−07	−5.037 8 e−07	−5.603 5 e−07
$\dot{z}_{\rm rel}$/(m/s)	−1.557 9 e−06	−1.325 0 e−06	−4.368 8 e−06	−1.963 6 e−06
Error/%	4.118 5	5.860 5	1.482 3	6.527 8

Among them, in the four results of Case 1, the minimum error is about 1.6%, the maximum is 70.2%, and the average error is about 40%. For Case 2, the minimum is about 5.7%, the maximum is about 19.1%, and the average is about 14%. For Case 3, the minimum is about 1.5%, the maximum is about 6.5%, and the average is about 4.5%.

Each optimization search will select an individual with the minimum value of the optimization function as the optimal solution. Under the same conditions, each simulation result will be different, which is caused by the high randomness of the DE algorithm and the random generation of initial populations and mutation vectors under the condition of satisfying the search range. However, under different simulation conditions, the differences of simulation results themselves are different, which is determined by the degree of nonlinearity under different relative orbit conditions. Generally, the further the relative distance is, the greater the orbital altitude difference is. Then a higher degree of nonlinearity can be provided, and the better observability is achieved. The initial relative distance of Case 2 is farther than that of Case 1, and the orbital altitude difference of Case 3 is greater than that of Case 1, the corresponding optimization results are better than that of Case 1.

7.3 LEO cases

It is assumed that the Chief is orbiting like the space station in LEO zone while the Deputy fly by the Chief that both of the vehicle are co-plane with different altitudes and phases. The orbit parameters are shown in Table 6. The relative distance at the initial epoch is less than 100 km. Cases with different measurement spans are tested in this subsection: 600 s, 1 200 s, 1 800 s, 2 400 s, 3 000 s, and 3 600 s. Ten simulation runs with same parameters are conducted for each case. In addition, the guess for the feasible solution search space is as shown in Table 7.

Table 6 Parameters setting of Chief and Deputy

Orbital element	Chief	Deputy
Semi major axis/m	6 731 140	6 771 140
Eccentricity	0.000 212	0.000 212
Inclination/(°)	41.471	41.471
Right ascension of ascending node/(°)	281.996 2	281.996 2
Argument of perigee/(°)	349.157 1	349.157 1
True anomaly/(°)	269.313 4	277.313 4

Table 7 Setting of feasible solution space guess

Relative state	Minimum	Maximum
ρ_{rel}/m	10 000	180 000
θ_{rel}/rad	-0.1α	0.1α
z_{rel}/m	−2 000	2 000
$\dot{\rho}_{\mathrm{rel}}$/(m/s)	−20	20
$\dot{\theta}_{\mathrm{rel}}$/(rad/s)	$-0.000\,01\alpha$	$0.000\,01\alpha$
$\dot{z}_{\mathrm{rel}}$/(m/s)	−20	20

The simulation results are shown in Table 8 where 10 runs are conducted for each case. It can be seen that the IROD solutions with different percentage errors of all cases are obtained. For Case 1, the minimum error is less than 0.4% while the maximum is 18.5%; for Case 2, the corresponding data are 7.6% and 19.6% while 0.3% and 22.1%, 0.4% and 36.9%, 1% and 34.6%, 1.1% and 30.6% respectively for Case 3 to Case 6. The statistics for all these data is presented in Fig. 4. As depicted in Fig. 4, a more accurate IROD solution is generally achieved when the measurement span is only 600 s, which is the least of all the cases. This means 30 measurements in 600 s could provide enough information for the LEO IROD in cylindrical coordinates. Moreover, the reason for the larger span worse performance is in the accuracy of the relative dynamics. As shown in Section 4, the state transition matrix is used in the IROD model. However, the state transition matrix is linear solution for the relative dynamics that high-order terms have been ignored, which leads to that the accuracy of the dynamics would be degraded when the span is larger.

Table 8 Percentage error of IROD solutions %

Case	Run #1	Run #2	Run #3	Run #4	Run #5	Run #6	Run #7	Run #8	Run #9	Run #10
1	10.5	18.5	11.4	12.1	14.3	16.7	1.7	2.9	0.4	0.9
2	13.0	14.0	14.5	16.9	7.6	8.4	16.4	9.0	20.8	19.6
3	3.3	4.2	22.1	11.9	14.3	19.9	0.3	8.8	3.8	28.5
4	1.2	2.7	4.0	12.8	0.4	12.9	33.3	7.3	30.1	36.9
5	1.0	3.5	10.3	13.4	13.3	14.5	2.3	34.6	12.1	12.0
6	21.3	25.3	1.1	30.6	5.8	6.4	22.1	5.5	5.6	29.5

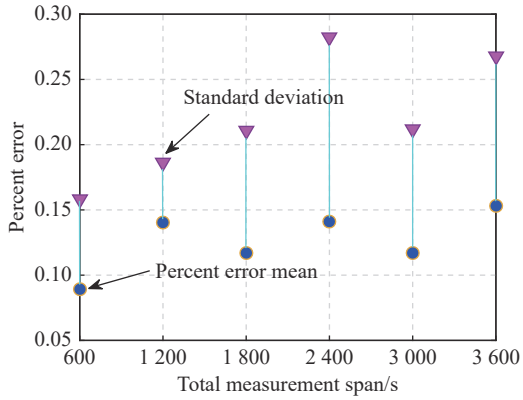

Fig. 4 Statistics for LEO simulation cases

These results are quite inspiring that the using of the cylindrical dynamics does provide the angles-only observability and the IROD solution with an appropriate accuracy can be achieved to initialize the navigation filter in a relative short span. Anyway, the problem of how short the measurement span can still lead to acceptable IROD solution should be studied further in the future.

8. Conclusions

In this paper, an angles-only initial relative orbit determination algorithm based on DE is developed for passive detection task of space non-cooperative targets. By introducing the relative dynamics in cylindrical coordinates, the state observability for the angles-only problem is confirmed by mathematically proven. The IROD frame for the case that Chief orbits circular trajectory, is constructed and solved by using the improved DE algorithm. The theoretical results are validated by numerical simulation where two different altitude orbits are included, i.e., GEO and LEO. The simulation results show the IORD solution could be obtained for both orbit types. For GEO cases, a larger measurement span is required for capturing orbital curvature to provide observability, while the span within 600 s is satisfied.

In the future, different perturbations will be considered and modeled in cylindrical dynamics, which may improve the angles-only observability. The sensitivity of the factors such as sensor accuracy and formation geometry to the IROD solution will be checked further.

References

[1] GONG B C, WANG S, LI S, et al. Review of space relative navigation based on angles-only measurements. Astrodynamics, 2023, 7(2): 131–152.
[2] GAIAS G, ARDAENS J S. In-orbit experience and lessons learned from the AVANTI experiment. Acta Astronautica, 2018, 153: 383–393.
[3] D'AMICO S, ARDAENS J, GAIAS G, et al. Noncooperative rendezvous using angles-only optical navigation: system design and flight results. Journal of Guidance, Control, and Dynamics, 2013, 36(6): 1576–1595.
[4] FLORES-ABAD A, MA O, PHAM K, et al. A review of space robotics technologies for on-orbit servicing. Progress in Aerospace Sciences, 2014, 68: 1–26.
[5] DAVID B. The phoenix project. https://www.unoosa.org/pdf/pres/stsc2013/tech-11E.pdf.
[6] CHARI R. Autonomous orbital rendezvous using angles-only navigation. Cambridge: Massachusetts Institute of Technology, 2012.
[7] CHEN T, XU S J. Approach guidance with double-line-of-sight measuring navigation constraint for autonomous rendezvous. Journal of Guidance, Control, and Dynamics, 2011, 34(3): 678–687.
[8] HIPPELHEUSER J, ELGOHARY T A. Inertial space-based orbit estimation: a new measurement model for multiple observers. Acta Astronautica, 2021, 181: 717–732.
[9] HIPPELHEUSER J, ELGOHARY T. A novel approach for initial orbit determination for space-based observation networks. Proc. of the 3rd IAA Conference on Space Situational Awareness, 2022: IAA-ICSSA-20-00-19.
[10] TASIF T H, HIPPELHEUSER J E, ELGOHARY T A. Analytic continuation extended Kalman filter framework for perturbed orbit estimation using a network of space-based observers with angles-only measurements. Astrodynamics, 2022, 6(2): 161–187.
[11] LEGRAND K, DEMARS K, PERNICKA H. Bearings-only initial relative orbit determination. Journal of Guidance, Control, and Dynamics, 2015, 38(9): 1699–1713.
[12] WANG Z W, GONG B C, YUAN Y H, et al. Incomplete information pursuit-evasion game control for a space non-cooperative target. Aerospace, 2021, 8(8): 211.
[13] ANDREWS B A, GELLER D K. Analysis of angles-only hybrid space-based/ground-based approach for geosynchronous orbit catalog maintenance. The Journal of the Astronautical Sciences, 2022, 69: 473–510.
[14] WOFFINDEN D C, GELLER D K. Observability criteria for angles-only navigation. IEEE Trans. on Aerospace and Electronic Systems, 2009, 45(3): 1194–1208.
[15] WOFFINDEN D C, GELLER D K. Optimal orbital rendezvous maneuvering for angles-only navigation. Journal of Guidance, Control, and Dynamics, 2009, 32(4): 1382–1387.
[16] GRZYMISCH J, FICHTER W. Observability criteria and unobservable maneuvers for in-orbit bearings-only navigation. Journal of Guidance, Control, and Dynamics, 2014, 37(4): 1250–1259.
[17] GRZYMISCH J, FICHTER W. Analytic optimal observability maneuvers for in-orbit bearings-only rendezvous. Journal of Guidance, Control, and Dynamics, 2014, 37(5): 1658–1664.
[18] GRZYMISCH J, FICHTER W. Optimal rendezvous guidance with enhanced bearings-only observability. Journal of Guidance, Control, and Dynamics, 2015, 38(6): 1131–1140.
[19] ANJALY P, RATNOO A. Observability enhancement of maneuvering target with bearings-only information. Journal of Guidance, Control, and Dynamics, 2018, 41(1): 184–198.
[20] PI J, BANG H. Trajectory design for improving observability of angles-only relative navigation between two satellites. The Journal of the Astronautical Sciences, 2014, 61: 391–412.
[21] HEBERT L. Angles-only initial relative-orbit determination via maneuver. Auburn: Auburn University, 2016.
[22] HOU B, WANG D Y, WANG J Q, et al. Optimal maneuvering for autonomous relative navigation using monocular camera sequential images. Journal of Guidance, Control, and Dynamics, 2021, 44(11): 1947–1960.

[23] LUO J J, GONG B C, YUAN J P, et al. Angles-only relative navigation and closed-loop guidance for spacecraft proximity operations. Acta Astronautica, 2016, 128: 91–106.
[24] ZHANG Y J, WANG J Q, HOU B W, et al. Optimal maneuvering strategy of spacecraft evasion based on angles-only measurement and observability analysis. Journal of Systems Engineering and Electronics, 2023, 34(1): 172–184.
[25] KLEIN I, GELLER D K. Zero Δv solution to the angles-onlyrange observability problem during orbital proximity operations. Proc. of the Bar-Itzhack Memorial Symposium on Estimation, Navigation, and Spacecraft Control, 2015: 351−369
[26] GELLER D K, PEREZ A. Initial relative orbit determination for close-in proximity operations. Journal of Guidance, Control, and Dynamics, 2015, 38(9): 1833–1841.
[27] GONG B C, GELLER D K, LUO J J. Initial relative orbit determination analytical covariance and performance analysis for proximity operations. Journal of Spacecraft and Rockets, 2016, 53(5): 822–835.
[28] GONG B C, LI W D, LI S, et al. Angles-only initial relative orbit determination algorithm for non-cooperative spacecraft proximity operations. Astrodynamics, 2018, 2(3): 217–231.
[29] GONG B C, LUO J J, LI S, et al. Observability criterion of angles-only navigation for spacecraft proximity operations. Proceeding of the Institution of Mechanical Engineers, Part G: Journal of Aerospace Engineering, 2019, 233(12): 4302–4315.
[30] CHRISTENSEN R, GELLER D. Spin-assisted angles-only navigation and control for SmallSats. Proc. of the 37th Annual AAS Guidance and Control Conference, 2014: AAS14-067.
[31] KAUFMAN E, LOVELL T A, LEE T. Nonlinear observability measure for relative orbit determination with angles-only measurements. The Journal of Astronautical Science, 2016, 63: 60–80.
[32] LOVELL T A, LEE T. Nonlinear observability for relative satellite orbits with angles-only measurements. Proc. of the 24th International Symposium on Space Flight Dynamics, 2014. https://issfd.org/ISSFD_2014/ISSFD24_Paper_S16-3_Lovell-pdf.
[33] NEWMAN B A, PRATT E, LOVELL A, et al. Quadratic hexa-dimensional solution for relative orbit determination. Proc. of AIAA/AAS Astrodynamics Specialist Conference, 2014. DOI: 10.2514/6.2014-4309.
[34] NEWMAN B A, LOVELL T A, PRATT E, et al. Hybrid linear-nonlinear initial determination with single iteration refinement for relative motion. Advances in the Astronautical Sciences, 2015, 155: 2149–2168.
[35] SHUBHAM G. Initial relative orbit determination using second order dynamics and line-of-sight measurements. Auburn: Auburn University, 2015.
[36] SHUBHAM G. Initial relative-orbit determination using second-order dynamics and line-of-sight measurements. Auburn: Auburn University, 2015.
[37] GONG B C, MA Y Q, ZHANG W F, et al. Deep-neural-network-based angles-only relative orbit determination for space non-cooperative target. Acta Astronautica, 2023, 204: 552–567.
[38] TOMBASCO J, AXELRAD P. Observability of relative hybrid elements, given space-based angles-only observations. Journal of Guidance, Control, and Dynamics, 2012, 35(5): 1681–1686.
[39] GAIAS G, D'AMICO S, ARDAENS J S. Angles-only navigation to a noncooperative satellite using relative orbital elements. Journal of Guidance, Control, and Dynamics, 2014, 37(3): 439–451.
[40] YIM J R, CRASSIDIS J L, JUNKINS J L. Autonomous orbit navigation of two spacecraft system using relative line of sight vector measurements. Proc. of the AAS/AIAA Spaceflight Mechanics Conference, 2004: AAS04-257.
[41] SULLIVAN J, D'AMICO S. Nonlinear Kalman filtering for improved angles-only navigation using relative orbital elements. Journal of Guidance, Control, and Dynamics, 2017, 40(9): 2183–2200.
[42] SULLIVAN J, LOVELL T A, D'AMICO S. Angles-only navigation for autonomous on-orbit space situational awareness applications. Proc. of the AAS/AIAA Astrodynamics Specialist Conference, 2018: AAS 18-468.
[43] ARDAENS J S, GAIAS G. A numerical approach to the problem of angles-only initial relative orbit determination in low earth orbit. Advances in Space Research, 2019, 63(12): 3884–3899.
[44] KOENIG A W, D'AMICO S. Observability-aware numerical algorithm for angles-only initial relative orbit determination. Proc. of the AAS/AIAA Astrodynamics Specialist Conference, 2020: AAS 20-594.
[45] GRZYMISCH J, FICHTER W, CASASCO M, et al. A spherical coordinate parametrization for an in orbit bearings-only navigation filter. Proc. of the 2nd CEAS Specialist Conference on Guidance, Navigation and Control, 2013: 215−231.
[46] GELLER D K, LOVELL T A. Non-iterative approximate solution to the angles-only initial relative orbit determination problem in spherical coordinates. Proc. of the 26th AAS/AIAA Space Fight Mechanics Meetings, 2016, 158: 356.
[47] PEREZ A C, GELLER D K, LOVELL T A. Non-iterative angles-only initial relative orbit determination with J2 perturbations. Acta Astronautica, 2018, 151: 146–159.
[48] GELLER D, LOVELL T A. Initial relative orbit determination performance analysis in cylindrical coordinates using angles-only measurements. Proc. of the 24th AAS/AIAA Space Flight Mechanics Meeting, 2014: AAS 14-212.
[49] GELLER D K, LOVELL T A. Angles-only initial relative orbit determination performance analysis using cylindrical coordinates. The Journal of the Astronautical Sciences, 2017, 64: 72–96.
[50] PEREZ A, LOVELL T A, GELLER D, et al. Relative satellite motion solutions using curvilinear coordinate frames. Proc. of the AAS/AIAA Astrodynamics Specialist Conference, 2015: AAS 15−437.
[51] GONG B C, ZHANG D G, ZHANG W F, et al. Angles-only relative navigation algorithm for space non-cooperative target in cylindrical frame. Journal of Chinese Inertial Technology, 2021, 29(6): 752–762.
[52] BILAL, PANT M, ZAHEER H, et al. Differential evolution: a review of more than two decades of research. Engineering Applications of Artificial Intelligence, 2020, 90: 103479.
[53] OPARA K R, ARABAS J. Differential evolution: a survey of theoretical analyses. Swarm and Evolutionary Computation, 2019, 44: 546–558.
[54] SI X G, BAO J D. Evaluate linearity error based on Hill-Climbing and differential evolutionary algorithm. Journal of Test and Measurement Technology, 2019, 33(5): 418–420.
[55] DENG W, SHANG S F, CAI X, et al. An improved differential evolution algorithm and its application in optimization problem. Soft Computing, 2021, 25(7): 5277–5298.

Biographies

DAI Chenchao was born in 1993. He received his B.S. degree from Rocket Force University. Currently, he is studying for his Ph.D. degree in Rocket Force University of Engineering. His research interests are multi-agent game confrontation and solid attitude-orbit control motor.
E-mail: dai32917zr@sina.com

QIANG Hongfu was born in 1965. He received his Ph.D. degree from Xi'an Jiaotong University. Currently he is a professor in Rocket Force University of Engineering. His research interests include agent game confrontation, structural integrity of solid rocket motor and advanced computational mechanics.
E-mail: Qiang@263.net

ZHANG Degang was born in 1997. He received his B.S. and M.S. degrees from Nanjing University of Aeronautics and Astronautics. His research interest is aerospace engineering.
E-mail: zdg765049828@qq.com

HU Shaolei was born in 1983. He received his M.S. degree from Xi'an Institute of Optics and Precision Mechanics. Currently, he is an engineer of Beijing Institute of Control and Electronic Technology. His research interest is navigation.
E-mail: hushaolei028@163.com

GONG Baichun was born in 1987. He received his Ph.D. degree from Northwestern Polytechnical University. Currently, he is an associate research fellow of Nanjing University of Aeronautics and Astronautics. His current research interests are space situational awareness and relative navigation for flight vehicles formation.
E-mail: baichun.gong@nuaa.edu.cn